

RSC Advances



This is an *Accepted Manuscript*, which has been through the Royal Society of Chemistry peer review process and has been accepted for publication.

Accepted Manuscripts are published online shortly after acceptance, before technical editing, formatting and proof reading. Using this free service, authors can make their results available to the community, in citable form, before we publish the edited article. This *Accepted Manuscript* will be replaced by the edited, formatted and paginated article as soon as this is available.

You can find more information about *Accepted Manuscripts* in the [Information for Authors](#).

Please note that technical editing may introduce minor changes to the text and/or graphics, which may alter content. The journal's standard [Terms & Conditions](#) and the [Ethical guidelines](#) still apply. In no event shall the Royal Society of Chemistry be held responsible for any errors or omissions in this *Accepted Manuscript* or any consequences arising from the use of any information it contains.

Silarylene-containing oligo(ether-amide)s based on bis(4-(4-amino phenoxy)phenyl)dimethylsilane. Effect of dicarboxylic acid structure on some properties

Claudio A. Terraza^{*1a}, Luis H. Tagle¹, Alain Tundidor-Camba¹, Carmen M. González-Henríquez², Deysma Coll¹ and Mauricio M. Sarabia^{1b}

¹ Pontificia Universidad Católica de Chile, ^a Facultad de Química, ^b Instituto de Física, P.O. Box 306, Correo 22, Santiago, Chile. ² Universidad Tecnológica Metropolitana, Facultad de Ciencias Naturales, Matemáticas y del Medio Ambiente, P.O. Box 9845, Correo 21, Santiago, Chile

Oligo(ether-amide)s (**PEAs**) based on diphenylsilane and oxyphenyl units were synthesized through Yamazaki-Higashi phosphorylation polyamidation technique. Thus, three new aromatic monomers were synthesized and characterized: a di(ether-amine), bis(4-(4-aminophenoxy)phenyl)dimethylsilane, and two dicarboxylic acids, bis(4-(4-carboxy phenoxy)phenyl)dimethylsilane and bis(4-(4-carboxyphenoxy)phenyl)diphenylsilane. MALDI-TOF mass spectrometry analyses show that average molecular masses of the **PEAs** ranged from 1334 to 2097 m/z. UV-vis technique was used to determine the optical band gap (E_g) of the oligomers. These values were between 3.91 and 4.57 eV. On the other hand, the conductivity of the samples was measured in solid state (film) through the “four point method” showing a slightly conductor behavior (13.3 and 5.0 Scm^{-1}). Determination of fluorescence emission peaks

showed two absorption bands. The first peak is related to a lesser electron-donating nature from an amide group, while the second peak was attributed to the polar solvent. Raman spectroscopy was used to determine the functional group in order to corroborate the structure and the crystallinity degree of the **PEAs**. Microstructural analyses of the samples were developed by using grazing incidence X-ray diffraction, showing amorphousness in the system studied. AFM micrographs showed that all the samples present certain porosity. On the other hand, the incorporation of flexibilizing oxyether linkages affected positively the solubility of the **PEAs** in common organic solvents, and also decreased significantly the values of glass transition temperature (T_g) and increased the transparency in the UV-vis region. In all cases, the thermal decomposition temperature values ($TDT_{10\%}$) were above 400 °C.

* To whom all correspondence should be send: E-mail: cterraza@uc.cl (C.A. Terraza)

Introduction

Condensation polymers are materials with wide applications in several fields of the industry. Specifically, aromatic poly(amide)s (PAs) present excellent mechanical, electrical and chemical properties.^{1,2} However, some specific industrial applications depend largely on the solubility properties and the useful range of temperature expressed as the difference between the glass transition temperature (T_g) and the thermal decomposition temperature (TDT).

Design and synthesis of monomers with structural modifications, such as the incorporation of bulky groups and flexible moieties, heterocycles and/or heteroatoms in general into the macromolecular backbone, promote excellent solubility in organic polar solvents and a

decrease of the T_g values, maintaining still a good thermal stability.³⁻⁵ Bruma *et al.*⁶ have described that the introduction of silicon atoms in the form of silylene moieties [-Ar-Si(R₁R₂)-Ar-] in aromatic polymers improve their solubility maintaining a high thermal stability. Likewise, the Ph-Si-Ph unit could participate on the electronic transport into conjugated polymeric chain, due to the interaction between the vacant *d*-orbitals of the silicon atom and the π -orbital of neighbour aromatic systems, opening this way the optoelectronic materials field for these kinds of polymers.

Many aromatic diamines based on carbon atoms have been prepared, characterized and used for obtaining several nitrogen-containing condensation polymer families. Also, there are various kinds of condensation copolymers based in similar diamines and their properties are discussed in numerous reports. Pratt *et al.*⁷ were the first to publish the synthesis of diamines with silicon as central atom bonded to four carbon atoms (H₂N-Ph-Si(R₁,R₂)Ph-NH₂). The authors reported that when R₁= R₂= methyl, the diamine undergoes a fast thermal decomposition. The stability of these compounds is increased with the replacement of one or both methyl groups by phenyl rings. From these works, several polymerizations have been developed with diamines containing diphenylsilane unit (Ph-Si-Ph), where the silicon atom is bonded to combinations of R₁ = methyl and R₂ = phenyl⁸ as well as R₁ = R₂ = methyl^{6,9} or phenyl.^{6,9-20} On the other hand, the inclusion of ether linkages into the chain of PAs has been explored by several research groups. Thus, diverse difunctional monomers have been synthesized and the properties of the derived polymers were established, with special attention to the solubility and their thermal parameters.^{21,22} Our group has also reported the synthesis, characterization and use of a diamine containing a diphenylsilane unit, where the silicon atom is bonded to combinations of R₁ = R₂ =

phenyl, R_1 = methyl and R_2 = ethyl or R_1 = methyl and R_2 = phenyl, incorporating also two oxyphenyl units in the structures. These aromatic diamines have been used in the preparation of a series of oligo(ether-amide)s, which properties were related to the specific structure of the monomers.²³⁻²⁵

In this work, we report the synthesis and characterization of three new difunctional compounds; a diamine and two dicarboxylic acids, all of them containing a diphenylsilane moiety and two oxyphenyl units in their structure. The others two substituted groups bonded to silicon atoms are methyl or phenyl for the diacid monomers and dimethyl for the diamine. From these monomers, **PEAs** were obtained by direct polycondensation reaction and their properties were determined using different techniques. Results were compared with those obtained from a silicon-containing PA without ether linkage into the main chain and the nature of the substituted groups bonded to the silicon atom from dicarboxylic acid moiety was related to the observed specific properties.

Experimental part

Materials

N,N'-dimethylformamide (DMF), anhydrous K_2CO_3 , 1-fluoro-4-nitrobenzene, 4-fluorobenzonitrile, hydrazine monohydrate, Pd/C activated (10 wt. %), toluene, *N*-methyl-2-pyrrolidone (NMP), triphenylphosphite (TPP) and pyridine (Py) were obtained from Aldrich Chemical (Milwaukee, WI). Calcium chloride anhydrous powder was purchased from Merck. Bis(4-hydroxyphenyl)dimethylsilane (**1**), bis(4-hydroxyphenyl)diphenylsilane (**2**) and bis(4-carboxyphenyl)dimethylsilane (**3**) were

previously synthesized in our laboratory^{26,27}. All other reagents and solvents were purchased commercially as analytical-grade and used without further purification.

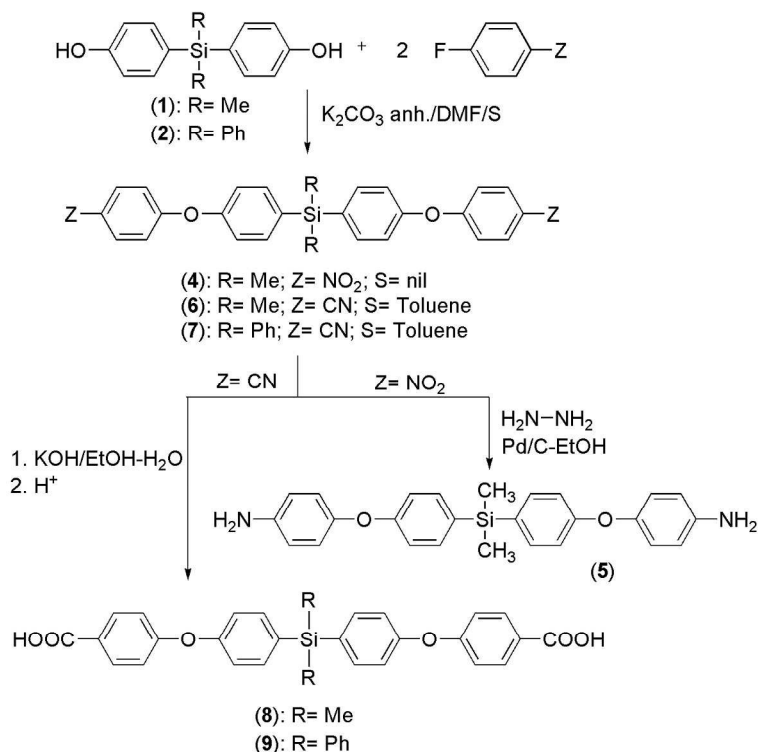
Measurements

FT-IR spectra (KBr pellets) were recorded on a Perkin-Elmer (Fremont CA) 1310 spectrophotometer over the range of 450-4000 cm^{-1} . ^1H , ^{13}C and ^{29}Si NMR spectra were carried out on a 400 MHz instrument (Bruker AC-200) using CDCl_3 or $\text{DMSO-}d_6$ as solvent and TMS as internal standard. Viscosimetric measurements were made in a Desreux-Bischof type dilution viscosimeter at 25 °C ($c = 0.5 \text{ g/dL}$). Tg values were obtained with a Mettler-Toledo (Greifensee, Switzerland) DSC 821 calorimetric system (10 °C min^{-1} under N_2 flow) after second heating run. Thermogravimetric analyses were carried out in a Mettler (Switzerland) TA-3000 calorimetric system equipped with a TC-10A processor, and a TG-50 thermobalance with a Mettler MT5 microbalance. Samples of 6-10 mg were placed in an alumina sample holder. Thermogravimetric measurements were carried out between 25 °C and 900 °C with a heating rate of 10 °C min^{-1} under N_2 flow. Elemental analyses were made on a Fisons EA 1108-CHNS-O equipment. UV-visible optical transmission spectra were obtained on a UV-3101PC UV-Vis-NIR scanning spectrophotometer (Shimadzu, Japan) at room temperature using solutions of NMP ($c = 5.0 \text{ g/L}$). Mass spectra (m/z) of the oligomers were obtained on a Microflex MALDI-TOF (Bruker Daltonics Inc., MA, USA) operated in the reflection mode for positive ions. Each **PEA** was mixed with the acid matrix α -cyano-4-hydroxycinnamic (CHCA) in 1:1 mol/mol ratio and 1 μL of each mixture was placed in a micro sample holder plate (Bruker Daltonics Inc., MA, USA) and slowly dried to allow polymer/matrix co-crystallization. Additionally, the spectra calibration was performed with external standard equipment for a

mixture of peptide masses 1000-3000 Da (Bruker Daltonics Inc., MA, USA). To control the spectrometer the software FlexControl 3.0 (Bruker Daltonik GmbH, Germany) was used. Spectra were acquired at different m/z intervals as sum of 20 scans of 30 laser impacts applied at different points taken at random from each sample placed in the sample holder plate. Absorption spectra were recorded from THF solutions ($c = 0.05$ mg/mL) at 25 °C with an Agilent 8453 diode array spectrophotometer and the band gap energy (E_g) was calculated from the adsorption edges. The same solutions were used for fluorescence measurements, which were obtained by a Perkin Elmer (Model LS-55) luminescence spectrometer equipped with a 7.3 W/50Hz xenon source. The parameters used were the following: Ex slit (nm): 5.0, Em. Slit (nm): 5.0, Scan speed (nm/min): 300 and the excitation were realized at 291 nm. For the conductivity studies thin films were prepared. To this purpose, **PEAs** samples were dissolved in THF and deposited by spin coating using rotation velocity ramps: 500 rpm about 10 s and 1600 rpm for 10 s on glass substrate at room temperature. Four-point electrical resistance measurements were applied to these films with the aim to obtain the system conductivity. Unpolarized Raman spectroscopy was performed with a LabRam 010 instrument from ISA using a 5.5 mW HeNe laser beam (633 nm) without filter. The Raman microscope uses a back-scattering geometry, where the incident beam is linearly polarized at 500:1 ratio. Microscope objective lens was an Olympus Mplan 100x, the integration time for each spectrum was 20 s with 10 accumulations. To this purpose, powder **PEA** was dissolved in THF and cast on glass slides, by spin coating technique using rotation velocity ramps: 500 rpm about 10 s and 1600 rpm for 10 s. Thin films were characterized by grazing incidence X-ray diffraction at room temperature with a Bruker D-8 Advanced Diffractometer, using an incident angle of 0.5° and a copper anode ($\lambda(\text{CuK}\alpha) = 0.154$ nm). The diffraction patterns were obtained in

the usual $\theta - 2\theta$ geometry and the diffracted X-rays were observed with a scintillation detector. Atomic force microscopy was used to analyze the superficial topography and holes deepness in the films. Toward this, the samples were dissolved in THF and put on a glass substrate. Measurements were performed with a Nanoscope IIIa equipment (formerly Digital Instrument, Inc., now Veeco Instrument, Inc) operating in contact mode. Tips were pyramidal shaped with 2 μm thickness; 450 μm length; 50 μm width; 13 Hz resonance frequency and 0.2 N/m force constant. To obtain the highest lateral resolution, an image was taken with 256 \times 256 pixels. Scanning of the sample was realized to the rate of one line collected per two seconds.

Silarylene-containing monomer synthesis



Scheme 1 Synthesis of the silarylene-containing monomers: bis(4-(4-aminophenoxy)phenyl)dimethylsilane (**5**), bis(4-(4-carboxyphenoxy)phenyl)dimethylsilane (**8**) and bis(4-(4-carboxyphenoxy)phenyl)diphenylsilane (**9**)

Bis(4-(4-nitrophenoxy)phenyl)dimethylsilane (4)

A mixture of 1.00 g (4.09 mmol) of **1**, 1.13 g (8.18 mmol) of anhydrous K₂CO₃, 1.15 g (8.18 mmol) of 1-fluoro-4-nitrobenzene and DMF (5 mL) was placed into a 50 mL flask with magnetic stirrer and condenser. The mixture was heated at 60 °C for 24 hours. On cooling, the mixture was poured into 600 mL of an ethanol-water solution (1:1 vol/vol) and a yellow solid was collected by filtration. Product was washed with hot ethanol-water and then dried at room temperature for 12 h to obtain 1.97 g (99 %) of a slightly yellow solid.

M.p.: 110-113 °C. IR (KBr, cm⁻¹): 3107, 3079 (C-H arom.), 2950 (C-H aliph.), 1597, 1579, 1487 (C=C arom); 1509, 1342 (NO₂); 1390, 1110 (Si-C arom.), 1312, 775 (Si-C aliph.), 1236 (C-O-C); 874 (arom. *p*-subst.). ¹H NMR (DMSO-*d*₆): 8.26 (d, *J*= 9.2 Hz, 4H), 7.66 (d, *J*= 8.5 Hz, 4H), 7.21 (d, *J*= 8.5 Hz, 4H), 7.16 (d, *J*= 9.2 Hz, 4H), 0.59 ppm (s, 6H). ¹³C NMR (DMSO-*d*₆): 162.4-117.7 (8C arom.), -2.6 ppm (Si-CH₃). ²⁹Si NMR (DMSO-*d*₆): -8.90 ppm. Elem. Anal. Calcd. for C₂₆H₂₂N₂O₆Si; (486.59): C, 64.17 %; H, 4.57 %; N, 5.76 %. Found: C, 63.76 %; H, 4.08 %; N, 5.58 %.

Bis(4-(4-aminophenoxy)phenyl)dimethylsilane (5)

A mixture of 1.50 g (3.08 mmol) of **4**, 0.37 g of Pd/C activated (10 wt. %) and 20 mL of ethanol was placed into a 100 mL three-necked flask fitted with magnetic stirrer, condenser and a dropping funnel. The system was heated to reflux and 18 mL of hydrazine monohydrate were added dropwise over a period of 1.5 hours. After the addition, the mixture was refluxed for 24 hours. The mixture was filtered and the solution poured into 800 mL of water with stirring. A white solid was obtained, which was filtered and dried at room temperature for 12 h to obtain 0.88 g (67 %).

M.p.: 86-89 °C. IR (KBr, cm^{-1}): 3402, 3333 (N-H), 3015 (C-H arom.), 2959 (C-H aliph.), 1619 (N-H flexion), 1587, 1508, 1493 (C=C arom); 1394, 1108 (Si-C arom.), 1311, 779 (Si-C aliph.), 1233 (C-O-C); 871 (arom. *p*-subst.). ^1H NMR (CDCl_3): 7.41 (d, $J= 8.5$ Hz, 4H), 6.83 (d, $J= 8.5$ Hz, 4H), 6.75 (d, $J= 8.7$ Hz, 4H), 6.58 (d, $J= 8.7$ Hz, 4H), 3.49 (s, 4H, NH_2), 0.49 ppm (s, 6H). ^{13}C NMR (CDCl_3): 160.0-116.2 (8C arom.), -2.1 ppm (Si- CH_3). ^{29}Si NMR (CDCl_3): -7.68 ppm. Elem. Anal. Calcd. for $\text{C}_{26}\text{H}_{26}\text{N}_2\text{O}_2\text{Si}$; (426.58): C, 73.20 %; H, 6.14 %; N, 6.57 %. Found: C, 73.66 %; H, 5.80 %; N, 6.18 %.

Bis(4-(4-cyanophenoxy)phenyl)dimethylsilane (6)

A mixture of 1.00 g (4.09 mmol) of **1**, 1.13 g (8.18 mmol) of anhydrous K_2CO_3 , toluene (20 mL) and DMF (10 mL) was placed into a 100 mL flask and heated at reflux using a Dean-Stark trap to remove the water azeotropically. After complete removal of water, the solvent was distilled from the system and 0.990 g (8.18 mmol) of 4-fluorobenzonitrile was added. The mixture was refluxed for 24 h. On cooling, the mixture was poured into 600 mL of an ethanol-water solution (1:1 vol/vol) and a grey solid was collected by filtration. This material was washed with hot ethanol-water and then dried at room temperature for 12 h to obtain 1.73 g of product (95 %).

M.p.: 125-127 °C. IR (KBr, cm^{-1}): 3025 (C-H arom.), 2953 (C-H aliph.), 2225 (CN), 1606, 1583, 1493 (C=C arom.); 1390, 1109 (Si-C arom.), 1293, 774 (Si-C aliph.), 1242 (C-O-C); 872 (arom. *p*-subst.). ^1H NMR (DMSO- d_6): 7.85 (d, J = 8.8 Hz, 4H), 7.62 (d, J = 8.3 Hz, 4H), 7.16 (d, J = 8.4 Hz, 4H), 7.13 (d, J = 8.7 Hz, 4H), 0.57 ppm (s, 6H). ^{13}C NMR (CDCl_3): 119.2 (CN), 161.1-105.8 (8C arom.), -2.0 ppm (Si- $\underline{\text{C}}\text{H}_3$). ^{29}Si NMR (CDCl_3): -8.05 ppm. Elem. Anal. Calcd. for $\text{C}_{28}\text{H}_{22}\text{N}_2\text{O}_2\text{Si}$; (446.57): C, 75.31 %; H, 4.97 %; N, 6.27 %. Found: C, 74.68 %; H, 4.68 %; N, 6.08 %.

Bis(4-(4-cyanophenoxy)phenyl)diphenylsilane (7)

The synthetic route to obtain bis(4-(4-cyanophenoxy)phenyl)diphenylsilane was similar to the procedure described for preparing dicyano derivative **6**, replacing diphenol **1** by derivative **2**. Yield 57 %.

M.p.: 133-135 °C. IR (KBr, cm^{-1}): 3069, 3019 (C-H arom.), 2226 (CN), 1606, 1584, 1492 (C=C arom.); 1390, 1116 (Si-C arom.), 1246 (C-O-C); 872 (arom. *p*-subst.), 699 (arom. *mono*-subst.). ^1H NMR (DMSO- d_6): 6.91-7.48 ppm (m, 26H). ^{13}C NMR (DMSO- d_6): 117.9 (CN), 160.7-106.2 ppm (12C arom.). ^{29}Si NMR (DMSO- d_6): -14.55 ppm. Elem. Anal. Calcd. for $\text{C}_{38}\text{H}_{26}\text{N}_2\text{O}_2\text{Si}$; (570.71): C, 79.97 %; H, 4.59 %; N, 4.90 %. Found: C, 78.25 %; H, 4.38 %; N, 4.56 %.

Bis(4-(4-carboxyphenoxy)phenyl)dimethylsilane (8)

A mixture of 1.50 g (3.35 mmol) of **6**, 3.75 g (67 mmol) of KOH, 50 mL of ethanol and 50 mL of water was placed into a 150 mL flask and heated at reflux. The reflux was continued for about 2 days until the evolution of ammonia had ceased. The mixture was filtered and the filtrate was diluted with 50 mL of water and acidified by aqueous HCl (1:1

vol/vol) mixture until pH 2-3. The precipitate was filtered, washed with water and dried at room temperature for 12 h to obtain 0.97 g (60 %). The crude product was dissolved with aqueous NaOH and then recrystallized by addition of aqueous HCl until pH 2.

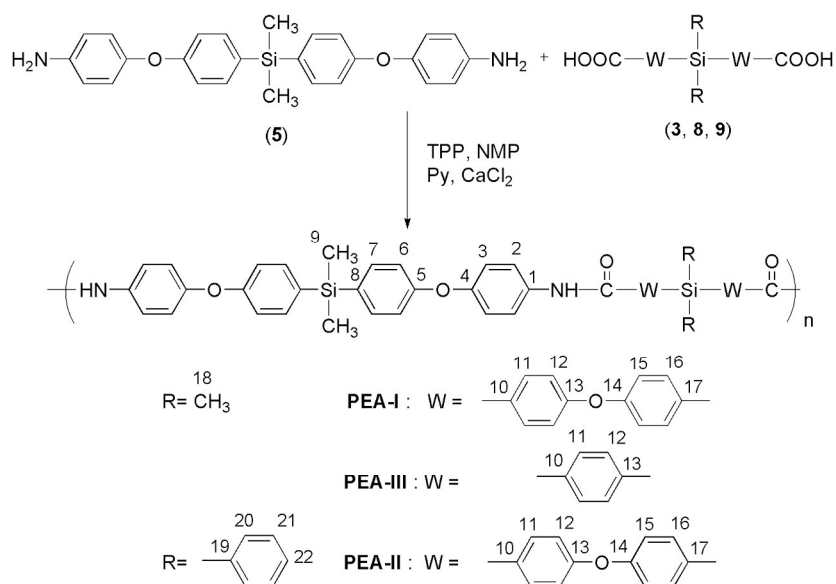
M.p.: 230-233 °C. IR (KBr, cm^{-1}): 3400 (O-H), 3075, 3019 (C-H arom.), 2956 (C-H aliph.), 1688 (C=O), 1607, 1585, 1494 (C=C arom.); 1108 (Si-C arom.), 1310, 774 (Si-C aliph.), 1242 (C-O-C); 874 (arom. *p*-subst.). ^1H NMR (DMSO- d_6): 7.96 (d, $J= 8.5$ Hz, 4H), 7.60 (d, $J= 8.1$ Hz, 4H), 7.12 (d, $J= 8.1$ Hz, 4H), 7.06 (d, $J= 8.5$ Hz, 4H), 0.56 ppm (s, 6H). ^{13}C NMR (DMSO- d_6): 167.2 (C=O), 160.9-118.1 (8C arom.), -2.0 ppm (Si- CH_3). ^{29}Si NMR (DMSO- d_6): -7.79 ppm. Elem. Anal. Calcd. for $\text{C}_{28}\text{H}_{24}\text{O}_6\text{Si}$; (484.57): C, 69.40 %; H, 4.99 %. Found: C, 68.89 %; H, 4.77 %.

Bis(4-(4-carboxyphenoxy)phenyl)diphenylsilane (9)

Bis(4-(4-carboxyphenoxy)phenyl)diphenylsilane was obtained following a similar procedure to that described for dicarboxylic acid **8**, using derivative **7** as precursor. Yield 70 %.

M.p.: 265-267 °C. IR (KBr, cm^{-1}): 3424 (O-H), 3068, 3023 (C-H arom.), 1688 (C=O), 1606, 1585, 1494 (C=C arom.); 1390, 1108 (Si-C arom.), 1243 (C-O-C); 874 (arom. *p*-subst.), 700 (arom. *mono*-subst.). ^1H NMR (DMSO- d_6): 12.90 (s, 2H, OH), 7.11-8.00 ppm (m, 26H). ^{13}C NMR (DMSO- d_6): 167.1 (C=O), 160.4-118.4 ppm (12C arom.). ^{29}Si NMR (DMSO- d_6): -14.34 ppm. Elem. Anal. Calcd. for $\text{C}_{38}\text{H}_{28}\text{O}_6\text{Si}$; (608.71): C, 74.98 %; H, 4.64 %. Found: C, 74.01 %; H, 4.56 %.

Oligo(ether-amides)s synthesis



Scheme 2 Synthesis of oligo(ether-amide)s by direct polyamidation

A typical polymerization procedure for the synthesis of the oligo(ether-amide)s was as follows.²⁸ A mixture of 0.47 mmol of **5**, 0.47 mmol of the corresponding dicarboxylic acid, 0.240 g of anhydrous CaCl₂, 0.3 mL of TPP, 1.2 mL of Py and 1.80 mL of NMP was heated with stirring at 110-120 °C for 3 hours. The mixture was poured in 300 mL of methanol with stirring. The white precipitate was filtered, washed thoroughly with

methanol and dried. The product was dissolved in DMSO and re-precipitated in methanol.

The solid was filtered and dried.

PEA-I: Yield: 89 %, $\eta_{inh} = 0.10$ dL/g (in DMSO at 25 °C, $c = 0.5$ g/dL), IR (KBr, cm^{-1}): 3421 (N-H), 3067 (C-H arom.), 2926 (C-H aliph.), 1647 (C=O), 1606, 1587, 1492 (C=C), 1407, 1014 (Si-C arom.), 1309, 777 (Si-C aliph.), 1228 (C-O-C), 874 (arom. *p*-sust.). 1H NMR (DMSO- d_6): 10.28 (s, 2H, NH), 8.03 (d, $J = 7.7$ Hz, 4H(11)), 7.83 (d, $J = 7.8$ Hz, 4H(2)), 7.51 (d, $J = 7.3$ Hz, 4H(7)), 7.45 (d, $J = 7.1$ Hz, 4H(12)), 7.19 (m, 8H(15,16)), 7.06 (d, $J = 8.1$ Hz, 4H(3)), 6.99 (d, $J = 7.3$ Hz, 4H(6)), 0.52 ppm (s, 12H(9,18)). ^{13}C NMR (DMSO- d_6): 164.5 (C=O), 159.6 (C13), 158.4 (C5), 155.5 (C14), 151.3 (C4), 135.6 (C16), 135.3 (C8), 131.4 (17), 130.1 (C7), 129.8 (C11), 129.4 (C10), 124.2 (C1), 121.9 (C2), 119.5 (C12), 119.4 (C15), 117.3 (C6), 117.0 (C3), -2.4 ppm (C9, C18). ^{29}Si NMR (DMSO- d_6): -8.98 ppm. Elem. Anal. Calcd. for $C_{54}H_{46}N_2O_6Si_2$; (875.12): C, 74.11 %; H, 5.30 %; N, 3.20 %. Found: C, 73.98 %; H, 5.18 %; N, 3.13 %.

PEA-II: Yield: 93 %, $\eta_{inh} = 0.20$ dL/g (in DMSO at 25 °C, $c = 0.5$ g/dL), IR (KBr, cm^{-1}): 3423 (N-H), 3068 (C-H arom.), 2954 (C-H aliph.), 1655 (C=O), 1606, 1585, 1492 (C=C), 1406, 1014 (Si-C arom.), 1308, 775 (Si-C aliph.), 1227 (C-O-C), 874 (arom. *p*-sust.), 700 (arom. *mono*-sust.). 1H NMR (DMSO- d_6): 10.25 (s, 2H, NH), 7.98 (d, $J = 6.9$ Hz, 4H(11)), 7.76 (d, $J = 8.0$ Hz, 4H(2)), 7.46 (m, 18H(12,20,21,22,7)), 7.12 (s, 8H(15,16)); 6.99 (s, 4H(3)), 6.91 (s, 4H(6)), 0.45 ppm (s, 6H(9)). ^{13}C NMR (DMSO- d_6): 165.0 (C=O), 159.2 (C13), 159.0 (C5), 158.0 (C14), 151.9 (C4), 138.3 (C20), 136.2 (C16), 136.1 (C7), 1357 (19), 133.9 (C8), 132.0 (C1), 130.4 (C22), 129.8 (C10), 128.9 (C17), 128.7 (C21), 122.5 (C2), 120.1 (C11), 119.1 (C12), 118.7 (C15), 117.6 (C6), 115.6 (C3), -1.9 ppm (C9). ^{29}Si NMR (DMSO- d_6): -8.12 (Si-diamine moiety), -15.04 ppm (Si-dicarboxylic acid moiety).

Análisis elemental. Calculado: $[C_{64}H_{50}N_2O_6Si_2]_n$ (999.26)_n: C, 76.93 %; H, 5.04 %; N, 2.80 %. Encontrado: C, 76.83 %; H, 4.98 %; N, 2.75%.

PEA-III: Yield: 75 %, $\eta_{inh} = 0.10$ dL/g (in DMSO at 25 °C, $c = 0.5$ g/dL), IR (KBr, cm^{-1}): 3427 (N-H), 3060 (C-H arom.), 2948 (C-H aliph.), 1654 (C=O), 1606, 1586, 1490 (C=C), 1410, 1103 (Si-C arom.), 1310, 773 (Si-C aliph.), 1226 (C-O-C), 874 (arom. *p*-sust.). 1H NMR (DMSO- d_6): 10.10 (s, 2H, NH), 7.70 (d, $J = 7.04$ Hz, 4H(11)), 7.57 (d, $J = 8.38$ Hz, 4H(2)), 7.45 (d, $J = 7.12$ Hz, 4H(12)), 7.25 (d, $J = 7.30$ Hz, 4H(7)), 6.81 (d, $J = 8.12$ Hz, 4H(3)), 6.73 (d, $J = 7.60$ Hz, 4H(6)), 0.38 (s, 6H(18)), 0.26 ppm (s, 6H(9)). ^{13}C NMR (DMSO- d_6): 167.8 (C=O), 157.8 (C5), 156.6 (C4), 150.8 (C8), 141.0 (C10), 135.0 (C12), 134.6 (C13), 133.2 (C11), 130.9 (C1), 126.2 (C7), 121.3 (C2), 119.0 (C6), 116.4 (C3), -3.1 (C18); -3.7 ppm (C9). ^{29}Si NMR (DMSO- d_6) -8.51 (Si-diamine moiety), -7.23 ppm (Si-dicarboxylic acid moiety). Elem. Anal. Calcd. for $C_{42}H_{38}N_2O_6Si_2$; (706.93): C, 71.35 %; H, 5.41 %; N, 3.96 %. Found: C, 71.14 %; H, 5.22 %, N, 3.57 %.

Results and discussion

Synthesis and spectroscopic characterization of monomers

Di(ether-amine) **5** was synthesized according to a procedure described previously^{23-25,29} (Scheme 1). The diphenolate was obtained from the silicon-containing compound **1**, which reacts with two equivalents of 1-fluoro-4-nitrobenzene by a nucleophilic aromatic substitution reaction. Then, the di(ether-nitro) derivative obtained is reduced by the action of the hydrazine-Pd/C system.

The FT-IR spectrum for di(ether-nitro) derivative **4** showed bands for N=O stretch at 1509 and 1342 cm^{-1} , also a signal at 1236 cm^{-1} corresponding to the C-O bending band. After

reduction, the nitro group absorption bands disappear and the N-H stretch ($3402, 3333 \text{ cm}^{-1}$) and N-H flexion (1619 cm^{-1}) bands appear. Figure 1a shows the ^1H and ^{13}C NMR spectra of diamine **5** in CDCl_3 solution. In the ^1H NMR spectrum, the signals at 0.49 and 3.47 ppm correspond to the protons of methyl and amino groups, respectively. On the other hand, the ^{13}C NMR spectrum exhibits eight peaks between 118 and 162 ppm due to the symmetry of the aromatic structure. The peak at -2.1 ppm corresponds to the methyl group bonded to the silicon atom, which appears at high field due to the low electronegativity of the silicon atom compared with that of carbon atom. Additionally, the structures of compounds **4** and **5** were confirmed by elemental analysis.

The dicarboxylic acids **8** and **9** were obtained according to a methodology similar to that used in the preparation of di(ether-amine) **5** (Scheme 1). 4-Fluorobenzonitrile was attacked by the corresponding silylated diphenolate, to obtain the dinitrile derivatives, which were converted into the respective dicarboxylic acids by alkaline treatment and later by acid hydrolysis.

Elemental analysis established a good correlation between the calculated and measured data for di(ether-nitrile) and dicarboxylic acid structures. For the di(ether-nitrile) derivatives, FT-IR spectra show bands associated to $\text{C}\equiv\text{N}$ stretch (2225 cm^{-1}) and to C-O bending (1246 cm^{-1}). After hydrolysis, the cyano group absorption bands disappear and the characteristic bands of O-H (3400 cm^{-1}) and C=O stretch (1688 cm^{-1}) appear. Figures 1b and 1c illustrate the ^1H and ^{13}C NMR spectra in $\text{DMSO}-d_6$ solution of the new dicarboxylic acids. ^1H NMR spectrum of **8** shows a signal at 0.56 ppm, corresponding to the methyl groups protons, and the signals between 7.05 and 7.97 ppm were associated to the *para*-substitution pattern on the benzene ring. Acidic proton was not observed. For the same compound, ^{13}C NMR spectrum exhibited the expected eight peaks corresponding to the

carbons of the aromatic rings and the peak at 167 ppm was assigned to the carbonyl carbon. A peak at high field (-1.98 ppm) corresponds to the $\text{CH}_3\text{-Si}$ moiety. On the other hand, in the ^1H NMR spectrum of **9**, the *para*-substitution pattern was unclear due to the presence of the phenyl groups hydrogen atoms bonded to the silicon atom. However, the acidic proton for this compound was observed at 12.90 ppm. The data for the ^{13}C NMR of **9** were consistent with the proposed structure in scheme 1.

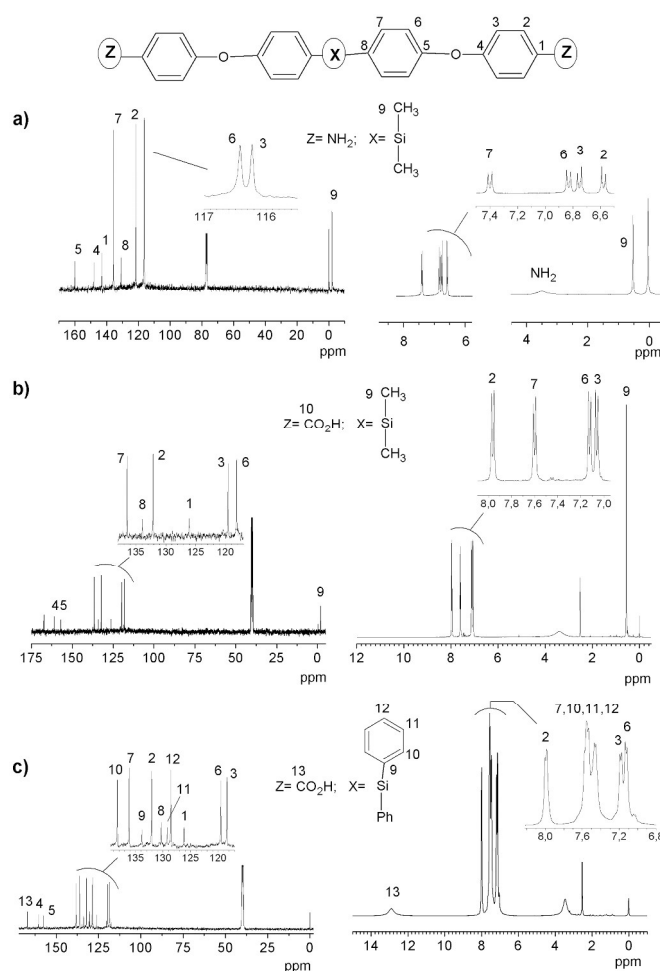


Fig. 1 400 MHz ^{13}C (left) and ^1H (right) NMR spectrum of new silylated monomers: diamine **5** (a), dicarboxylic acids **8** and **9** (b and c; respectively).

Synthesis and characterization of PEAs

Three new **PEAs** with yield between 75–93 % were prepared by the Yamasaki phosphorylation polyamidation methodology²⁸ (Scheme 2). **PEAs** structures were confirmed by elemental analysis and spectroscopic analyses.

FT-IR and NMR spectra

FT-IR spectra for **PEAs** showed a wide band at about 3420 cm^{-1} and other between 1647 and 1655 cm^{-1} , corresponding to the N-H and C=O amidic stretching, respectively. Near 1225 cm^{-1} the stretching band associated to the C-O-C ether unit is present. Additionally, at 1309 and 775 cm^{-1} the stretching bands for Si-C aliphatic bond appear while the Si-C aromatic linkage shows bands at 1497 and 1014 cm^{-1} . ^1H NMR spectra of all **PEAs** showed a signal at 10 ppm approximately, corresponding to the N-H amidic linkage. **PEA-I** spectra showed a peak at 0.52 ppm corresponding to methyl groups of both monomers moieties. Although these nuclei are not magnetically equivalent, their environments are very similar and, therefore, their chemical displacements are very close, appearing as a singlet that integrates for twelve H. **PEA-II** shows a signal at 0.44 ppm, corresponding to the methyl groups provided by the diamine moiety. However, in the **PEA-III** spectrum, this signal appears duplicated, maybe related to the environmental surroundings of silicon atoms in both monomers, which are magnetically different. The NMR ^{13}C spectra show the amide-carbonyl signal at 164-168 ppm. At higher field the aromatic carbons of the ether linkage appear while the methyl carbons bonded to silicon atom appear between -2.0 and -3.7 ppm,

approximately. An analysis of the ^{29}Si NMR spectra for all **PEAs** shows that the replacement of an aliphatic group by an aromatic ring shifts the silicon signal to a higher field. This phenomenon occurs because the aromatic ring induces a higher electron density on the silicon atom³⁰. In this same analysis **PEA-I** shows only one silicon signal since the magnetic environment of the monomers moieties are very similar, while **PEA-II** and **PEA-III** have two signals due to the different surrounding of silicon atoms in the chain.

Raman spectroscopy and crystallinity

Amide group usually has a C=O band in the region $1695\text{-}1630\text{ cm}^{-1}$ that is strong in the IR and weak in Raman³¹. Analysis of the spectra (Figure 2a) shows that all **PEAs** have a weak peak at 1650 cm^{-1} , approximately, related to this group. However, no spectrum shows the hydrogen-bonded NH band expected at 3300 cm^{-1} , probably due to its low intensity. A band between $1538\text{-}1550\text{ cm}^{-1}$ involves both C-N-H stretch and C-N-H bend in the stretch bend mode (amides II), which is characteristic for noncyclic mono substituted amides³²⁻³⁵. Additionally, the C-N-H stretch and C-N-H open are observed at $1260\text{-}1265\text{ cm}^{-1}$, approximately, with a broad band that possible could be coupled with the symmetric deformation of the methyl group in the Si-CH₃ moiety. Very-weak bands at $1410\text{-}1420\text{ cm}^{-1}$ would correspond to the respective antisymmetric deformation. Si-CH₃ rock is not observed with clarity due to band weakness, but possibly could be at $770\text{-}830\text{ cm}^{-1}$. On the other hand, the CH₃ vibration antisymmetric stretching corresponds to the frequencies observed at 2965 cm^{-1} , approximately. The C-H stretching vibrations of substituted benzenes usually give rise to IR and Raman bands in the $3100\text{-}3000$ region³⁶⁻³⁸. Thus, the phenyl groups presented only a weak band at $3050\text{-}3070\text{ cm}^{-1}$. On the other hand, the sharp

band at $1600-1610\text{ cm}^{-1}$, approximately, involves in-plane (*ip*) C-H bending vibrations that interact with various rings C-C vibrations. At about 1165 cm^{-1} , a tangentially moving carbon and its hydrogen usually move in opposite direction. Between $1105-1110\text{ cm}^{-1}$ it is possible to find a band associated to carbon and hydrogen moving in the same direction, overlapped with the out-of-plane (*oop*) C-H bending (or wag) vibrations of the benzene rings. In this sense, the band at $610-640\text{ cm}^{-1}$ corresponds to the movement of the hydrogen that usually is *oop* in the same direction. Characteristic frequencies of the ether function are due to the vibrations involving C-O linkages. Thus, the aryl-O bond is observed in all samples at 1320 cm^{-1} , approximately, with a weak intensity.

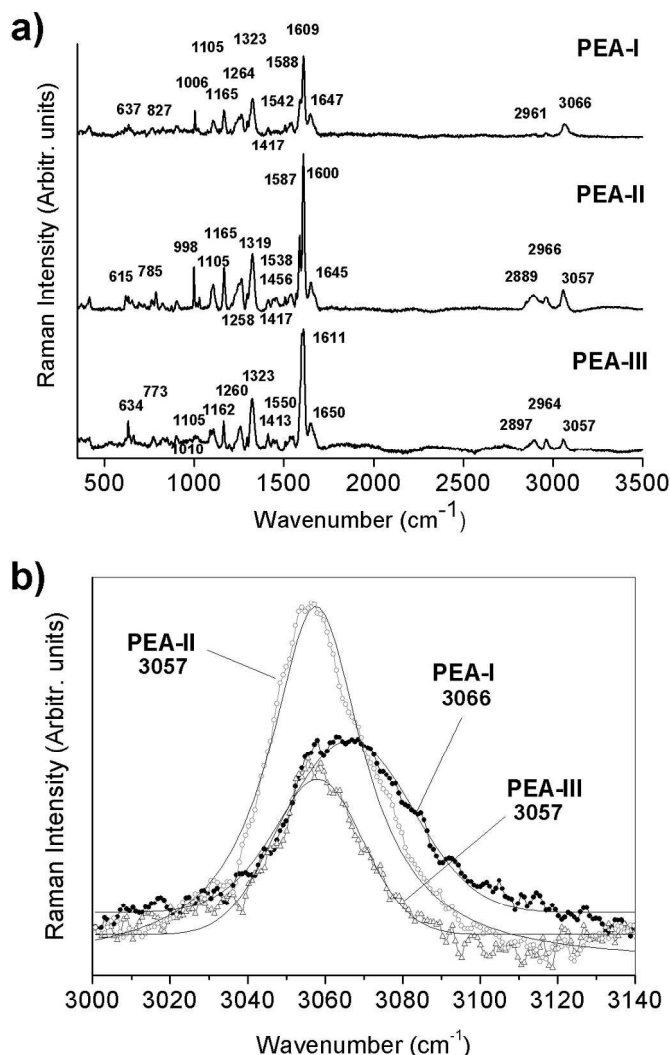


Fig. 2 a) Raman spectra of oligo(ether-amide)s at room temperature. b) Expansion for the 3000-3140 cm⁻¹ region of experimental spectra (line and symbol) and fitted spectra (continuous line).

Raman results were used to study the crystallinity of the oligomers. For this purpose, the peak near 3050 cm⁻¹, which shows good resolution by means a Gaussian function, was fitted (Figure 2b). Thus, the sigma parameter (σ) obtained for **PEA-I** is 16.07 centered at 3066 cm⁻¹; **PEA-II** is 29.45 and **PEA-III** is 11.83. For the two latter polymers this signal is centered at 3057 cm⁻¹. Sigma values (σ) obtained in the specific analyzed zone show that **PEA-III** has the highest structural order, without being crystalline, while **PEA-II** is the

most amorphous sample. These behaviors are possibly related to the intrinsic properties of the material and their structure. Thus, the packing forces in **PEA-III** are greater than those in its homologues due to the rigidity of the diacid moiety. Oxyether bonds in the same monomer for **PEA-I** and **PEA-II** promote a higher flexibility of the chains and, therefore, the amorphous regions are longer. The larger volumes of the phenyl rings, compared with methyl groups bonded to the silicon atom in the di(ether-amine) portion, promote a steric problem to the packing process of the chains in **PEA-II**.

Inherent viscosities and solubility of PEAs

Recovered inherent viscosities values (Table 1) were low. These indicate the formation of oligomeric chains, which was ratified by MALDI-TOF analyses. Solubility tests were developed for various organic solvents at room temperature. All samples were soluble in aprotic polar solvents, such as *m*-cresol and even in a low boiling point solvent such as THF. These results can be attributed to the inclusion of the ether linkages in the repetitive units, which increase the flexibility chain, reducing the packing effects and, therefore, allowing a better solvation of the material. In spite of the fact that all the samples were insoluble in CHCl₃ even when heated at 60 °C, the solubility shown in THF should increase the samples processability.

Table 1 Yields, inherent viscosity, solubility and cut-off wavelength of **PEAs**

Solvent ^b

	Yield (%)	η_{inh}^a (dL/g)	λ_{cutoff}^c (nm)	DMF	DMSO	DMAc	<i>m</i> -Cresol	NMP	THF	CHCl ₃
PEA-I	89	0.10	328	+	+	+	+	+	+	-
PEA-II	93	0.20	324	+	+	+	+	+	+	-
PEA-III	75	0.10	336	+	+	+	+	+	+	-

^a Values were taken from DMSO solutions ($c=0.5$ g/dL) at 25 °C. ^b Solubility: +, soluble at room temperature; -, insoluble at room temperature even with heating. ^c Recovered from NMP solution ($c=0.5$ g/L) at room temperature.

MALDI-TOF mass spectrometry

MALDI-TOF analyses were developed to establish **PEAs** molecular mass. Table 2 summarizes the observed m/z value for each sample and the proposed monomer sequence inside of the chains. Thus, m/z signals were assigned to protonated forms $[M+X^+]$ associated to average molecular masses ranging from 1334 to 2097 m/z . These results showed the formation of dimmers $(A-B)_2$ for all **PEAs** with different relative intensity measured as weight percentage. **PEA-I** also showed a peak associated to an A-B-A system that is formed by one full monomeric unit with an additional moiety of dicarboxylic acid, with a relative intensity of 32 %. On the other hand, **PEA-III** sample is also associated with a trimer unit.

Figure 3 represents a typical MALDI-TOF spectrum for these oligo(ether-amide)s. In this figure, **PEA-III** shows a series of intense peaks ranging from 1100 to 2500 Da, which are assigned to $[M+X^+]$ molecular ions. Two most intense peaks of this series correspond to oligomers with $n=2$ and $n=3$. These oligomers show values of 1454 m/z and 2084 m/z ,

Table 2 Structural assignment with its respective molecular mass for oligo(ether-amide)s detected by MALDI-TOF mass spectrometry

	Calculated A-B monomeric unit (g/mol)	m/z observed	Molecular mass (m/z)	Observed units
PEA-I	893	895	1334 and 1733	A-B-A and (A-B) ₂
PEA-II	1017	1079	2097	(A-B) ₂
PEA-III	709	1454	2084	(A-B) ₂ and (A-B) ₃

Moiety coming from: A= dicarboxylic acid and B= diamine.

respectively, with a low relative intensity for the latter signal (20.9 %). The spectrum also displays other mass peaks, which would be related to other oligomer series and/or to possible degradation products.

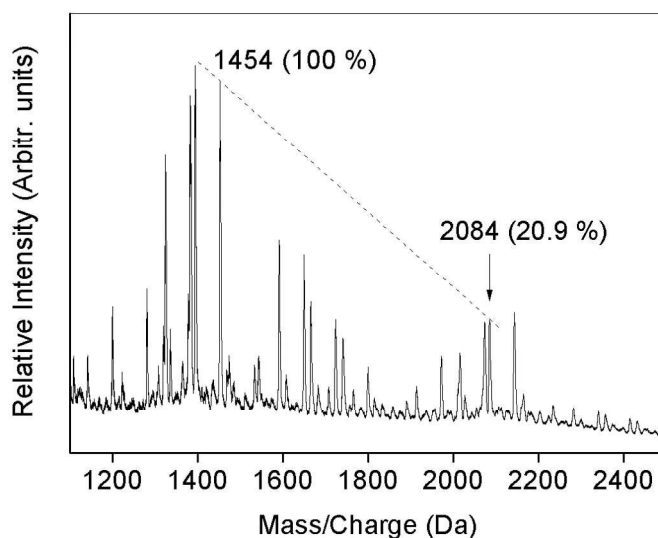


Fig. 3 MALDI-TOF spectrum of **PEA-III**, using a matrix α -cyano-4-hydroxycinnamic (CHCA).

Thermal properties

Glass transition temperatures (T_g), thermal decomposition temperatures ($TDT_{10\%}$) and residual weight values are summarized in table 3. Figure 4a shows the TGA thermograms of the samples. All samples had excellent thermal stability, **PEA-III** showing the lowest $TDT_{10\%}$ value. This result shows that the incorporation of phenyl moieties in the repetitive unit (-PhO-) favors the final thermal resistance of the materials. Thus, **PEA-II** had the highest $TDT_{10\%}$, which was expected due to the higher aromatic content of this sample. For this sample, two decomposition peaks appear on the TGA curve. Probably, the highest temperature peak corresponds to the rupture of the aromatic rings that are not part of the central chain. All samples show a percentage of residue even at 900 °C (16-33 %), which probably corresponds to silicon oxide.

Table 3 Thermal properties of **PEAs**

	$TDT_{10\%}$ ^a (°C)	Rw ^b (%)	T_g ^c (°C)
PEA-I	417	16	43
PEA-II	439	33	79
PEA-III	387	26	91

^a Thermal decomposition temperatures at which 10 % weight loss was obtained by TGA at a heating rate of 10 °C/min in nitrogen.

^b Residual weight (%) when the sample was heated to 900 °C at scan rate of 10 °C/min in nitrogen.

^c Glass transition temperature taken from the second heating scan (10 °C/min in nitrogen).

The effect of including the aryl ether units was observed markedly on the values of T_g (Figure 4b). **PEA-I** and **PEA-II** had T_g values lower than **PEA-III**. This fact confirms that the incorporation of flexible units in the backbone of the sample (-O-) increases the internal

mobility of the chain and, therefore, decreases the T_g values. Moreover, the higher T_g value for **PEA-II** compared with **PEA-I** is probably due to increased stiffness of the chain due to a higher aromatic content. Temperature range between T_g and TDT was very wide for all oligo(ether-amide)s, a desired feature for further processing.

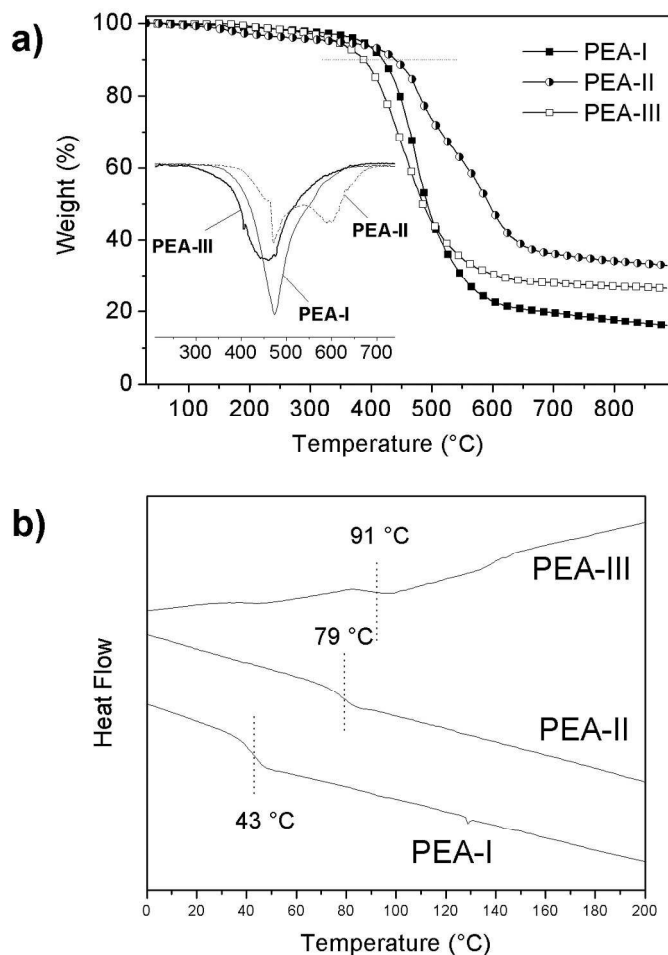


Fig. 4 DSC (a) and TGA (b) traces of oligo(ether-amide)s.

Optical and electrical properties

Optical transmission spectra (Figure 5) of all samples were obtained from NMP solution (5 g/L) at room temperature. Transmittances observed in the visible region are higher than 90 % at 400 nm, which allows classifying the **PEAs** as highly transparent materials. These results can be attributed to the presence of flexible ether linkages in the structure. Transparency depends, among other factors, on the conjugation of stacked benzene rings packing. When these conjugations take place, the π electrons will absorb energy from the visible-UV region. Incorporation of ether linkage to the oligo(ether-amide) main chains can reduce the conjugation due to the flexibility, which makes difficult the stacking of the benzene rings³⁹.

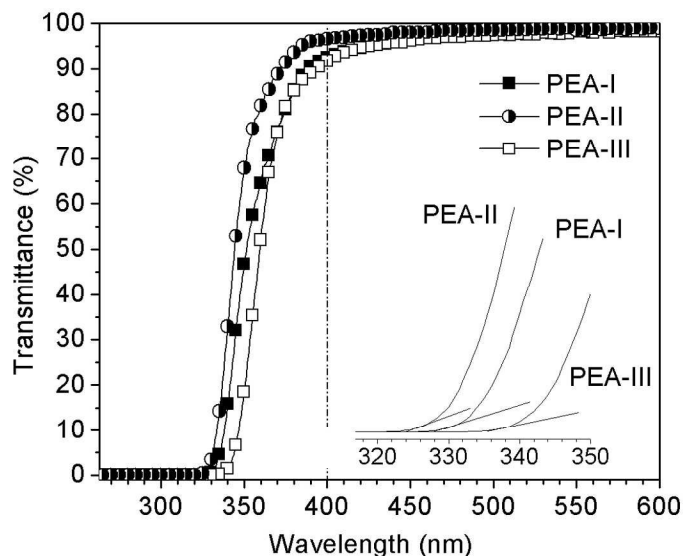


Fig. 5 UV-vis transmittance spectra of oligo(ether-amide)s at room temperature.

PEA-II shows greater transparency at 400 nm (96 %). This fact can be explained by larger volume of the benzene ring bonded to the silicon atom. This bulky group increases the separation between chains, reducing the inter- and intra-molecular charge transfer (CT)

complex formation. As a result, the π electrons in benzene rings will become hard to conjugate with other benzene rings, thereby improving the transmittance in the visible region. On the other hand, the λ_{cutoff} were estimated in the range of 320 to 332 nm (Table 1). **PEA-II** begins to be transparent before **PEA-I** and **PEA-III**, respectively. These two optical parameters makes the synthesized oligo(ether-amide)s possible candidates for applications in the optic-device field.

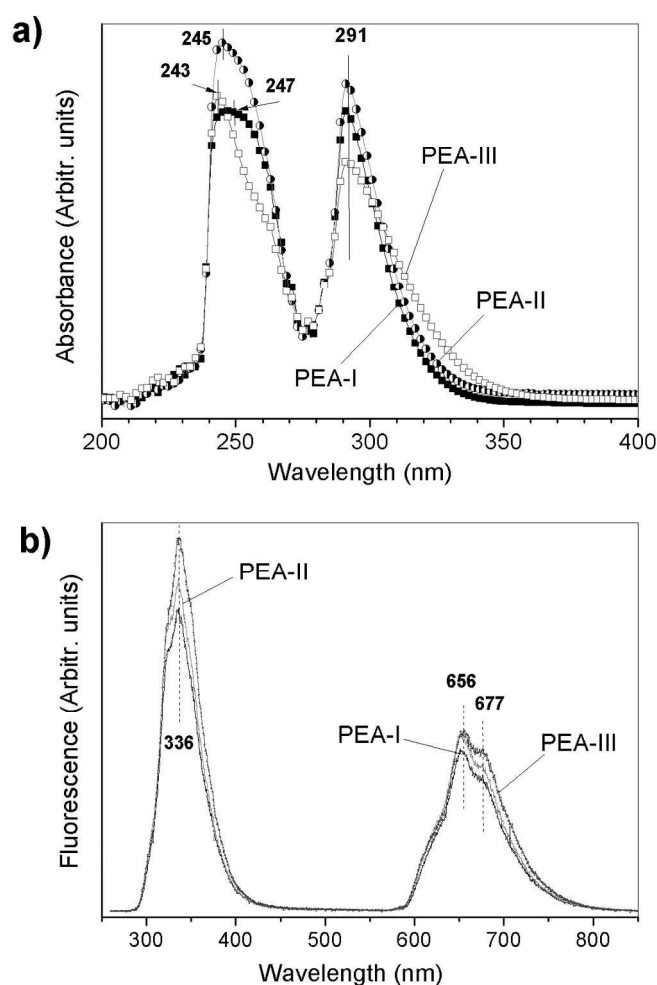


Fig. 6 Optical properties of oligo(ether-amide)s: a) UV-vis absorption and b) fluorescence spectra of **PEAs** in THF solution at room temperature.

Also, the optical properties of the samples were investigated in order to establish their absorption behavior (Figure 6a). All samples exhibited two strong absorption bands in THF solution, which are assigned to the n- π^* transition resulting from the conjugation between the aromatic rings and nitrogen atoms. The first band is centered between 243 and 247 nm, while the second band appears at 291 nm (Table 4). This behavior could also be favored by the intermolecular CT complexes formation. Although the chain flexibility diminishes the stacked packaging option, it would still be possible to visualize inter- and intra-chain interactions among electron-donor groups with sufficiently low ionization potential and acceptor units with high electron affinity.

Table 4 Optical and electrical behavior of the oligomers

	Optical Properties			Electrical Properties ^b	
	Absorption (λ_{\max} , nm)	Optical band gap ^a (Eg, eV)	Fluorescence (nm)	Resistance (Ω)	Conductivity (S/cm)
PEA-I	247 and 291	4.57	336, 656 and 677	0.3	13.3
PEA-II	245 and 291	4.57	336, 656 and 677	0.5	8.0
PEA-III	243 and 291	4.57	336, 656 and 677	0.8	5.0

^a Values associated to the band centered at 291 nm (Figure 6a).

^b Distance between the two measured points is 2.5 mm.

Optical band gap energy (Eg) in an extended system is defined as the difference between the lowest band energy in the conduction band and the highest band energy in the valence band. These values were obtained from the absorption spectra in the UV-vis range, using the Tauc's expression (Equation 1)^{40,41}. This equation includes a proportionality constant

(*b*) and the optical absorption coefficient (α), which determines the optical energy gap, as a function of the photon energy $h\nu$.

$$\alpha (h\nu)^2 = b (h\nu - E_g) \quad (1)$$

The optical absorption coefficient was calculated using equation 2, which corrects the reflection losses. Parameter A is the absorbance and l the square cell with an optical path length of 1 cm.⁴²

$$\alpha = 2.303 (A/l) \quad (2)$$

By plotting $(\alpha h\nu)^2$ versus $h\nu$, the direct gap was obtained from extrapolation of the linear portion of the plot for each sample⁴¹. Table 4 shows the values of band gap at 4.57 eV for all PEAs, which could be associated with an insulator behavior. Although the systems show different flexibility, the band gap values were not affected by this parameter. This fact could be associated to the high mobility of the chains in solution and, therefore, to a decrease in the coplanarity of the aromatic moieties.

Fluorescence emission spectra for the **PEAs**, carried out with an excitation source at 291 nm, showed a similar pattern composed by two signals (Figure 6b and Table 4). The first signal is an intense band centered at 336 nm, which is reasonable on the basis of the less electron-donating nature of the amide group. The second signal, of lower intensity, corresponds to two overlapped bands centered at 656 nm and 677 nm, respectively. These latter bands could be attributed to the solvent used in the spectral characterization due to its polar nature and, also, to the possibility to generate hydrogen bonds between the macromolecule and the solvent. This effect is detected as solvent molecules reorganization

(around of the fluorophore), producing a new type of distribution, and therefore, changing their molecular dipole moment.

Electrical conductivity measurements were carried out on solid films using the four-point technique and the results are shown in Table 4. All samples showed located and superficial conductivity between 13.3 and 5.0 Scm^{-1} , values associated to slightly conductor materials. Seemingly, in solid state the aromatic rings of the chains show a coplanarity higher than in solution. This result is in accordance with the sample structure since the conductivity is promoted by: (i) the presence of a conjugated double bond along the backbone, (ii) the possibility of interaction between the vacant *d*-orbitals of the silicon atom and the π system bonded to it, and (iii) the force of the phenyl group perpendicular to the main chain. All these structural characteristics favor the flux of charge in the form of extra electrons or “holes” injected into the material matrix.

It should be mention that the optical studies to measure the band gap previously discussed were realized in solution. Thus, the conductivity obtained in this case is completely different to that acquired by the four-point probe method developed on the films.

X-ray diffraction

Figure 7 presents grazing incidence X-ray diffraction (GIXRD) patterns of sample films at room temperature. The measurements realized within a range of $2\theta= 10-40^\circ$ showed in all cases amorphous structures, without the presence of peaks associated to planes diffraction. This fact would be associated to the interplanar distance promoted by the substituted groups bonded to the silicon atom and the flexibility shown by the chains. Thus, the non-preferred

orientation of the chains into of the oligomeric system would also be associated to its low molecular weight and/or to weak specific interaction between them.

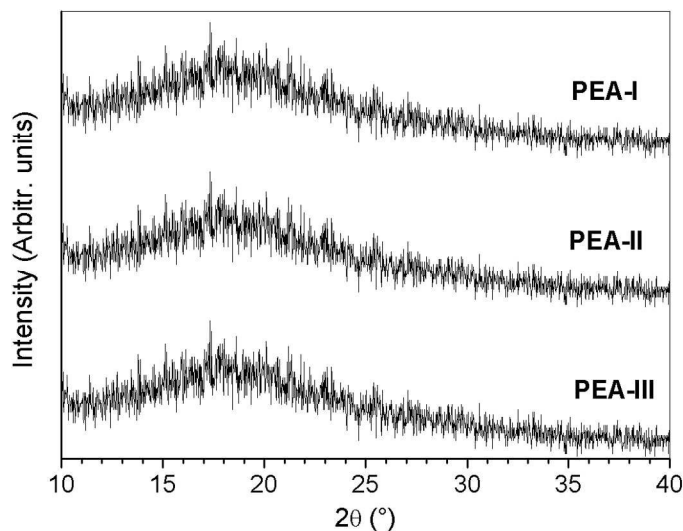


Fig. 7 GIXRD patterns of the films at room temperature.

Atomic Force Microscopy (AFM)

Topographic results of the oligo(ether-amide)s using AFM technique are shown in Figure 8. 3D images with X and Y dimensions of 50 μm and Z-scale variable appear to the left side, while 2D images (X and Y dimensions are both 50 μm) are shown to the right side. Deepness of the hole obtained in contact mode for the three **PEAs** are listed in Table 5. This parameter is determined through distance variations on the sample surface with a line traversing the image, as shown in each figure (right side). Thus, these data represent an accurate reflection of the variation of the surface topography of the samples.

Density and deepness of holes are very different for the three oligo(ether-amide)s. The deepness varies from 891 to 71 nm on an area of $50 \times 50 \text{ nm}^2$. Due to the fact that all

samples were prepared using the same methodology, the results indicate that the morphology of the **PEAs** was affected by the molecular weight of the oligomers and their specific structural details. We propose that an increase in the molecular mass of the material also increases the

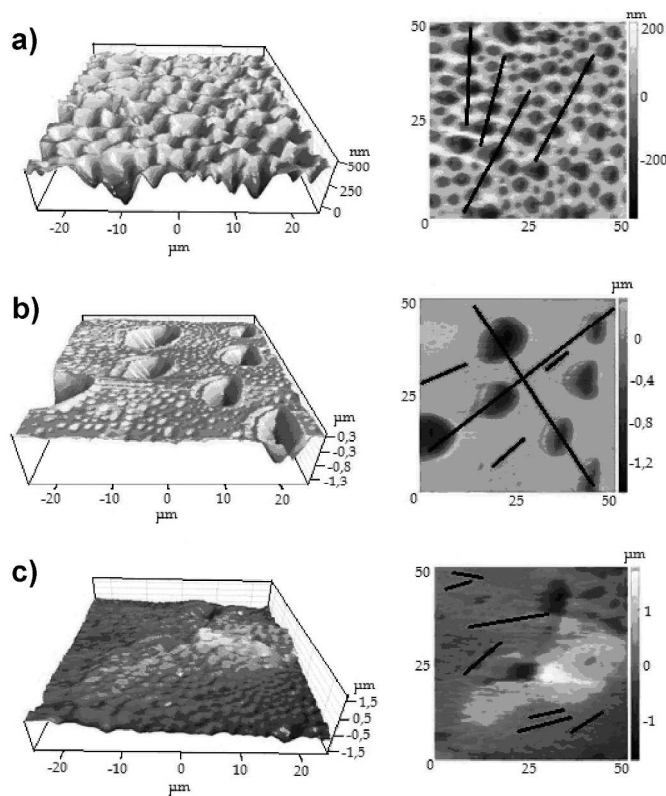


Fig. 8 3D (left) and 2D (right) topography images of oligo(ether-amide)s: a) **PEA-I**; b) **PEA-II** and c) **PEA-III**.

fraction of the occupied area. Thus, during the formation of the film, the oligomers with the highest m/z values would show highest affinity in the adsorption process (substrate), in accordance with their solubility and their corresponding diffusion coefficient compared with the chains of low m/z ratio. This fact would decrease the film height and therefore the deepness of their holes. The packing forces between chains also affect the thickness film.

PEA-III have the highest molecular weight and the lowest flexibility with methyl groups as lateral elements. These two facts promote the highest proximity between the chains with a minimum occupied volume for them during the process of formation of the film and therefore the observed holes present the lowest average deepness.

Table 5 Deepness of the holes at surface level obtained with contact AFM technique

	Average deepness of the holes (nm)	Error (nm)	Standard deviation
PEA-I	332.83	30.54	125.94
PEA-II	890.52 (great hole)	59.99	317.45
PEA-II	71.06 (small hole)	2.66	22.45
PEA-III	169.59	14.31	169.91

On the other hand, **PEA-II** without being the most flexible material or the sample of smallest molecular weight, has two phenyl groups bonded to one of the silicon atoms (dicarboxylic acid unit), which promotes a steric problem to the proximity of the chains. Due to this, it is evidence packaging forces of low intensity and therefore the height of the film is the highest one. In this case, the structural effect is more important than the chain molecular weight.

Conclusions

Three new oligo(ether-amide)s based on silarylene and oxyarene units were synthesized and spectroscopically characterized. All **PEAs** were soluble in several organic polar solvents even in THF. Inherent viscosity values and the results of MALDI-TOF analyses suggest the formation of oligomeric chains with sequences A-B, (A-B)₂ and (A-B)₃.

MALDI-TOF results also show other mass peaks that could be related to other oligomeric series or possible degradation products. In general, all **PEAs** can be classified as thermally stable due of the low weight loss above 400 °C. **PEA-I** and **PEA-II** had the higher decomposition temperature due to the high aromatic contribution. The incorporation of flexible units in the main chain decreases the Tg values and increases the transparency in the UV region.

Raman spectroscopy was also used to estimate the crystallinity or amorphousness of the **PEAs** through the Gaussian fit of the data with respect to a stretching characteristic band. Results were associated to the different packing forces that operate between the chains and therefore to the structural details of the respective repetitive units. The optical band gap (E_g) values estimated for the **PEAs** by UV-Vis spectroscopy show an insulator behavior in all cases. These results show that in solution, the flexibility shown for the chains affects negatively the planarity of the systems. However, the conductivity of the samples taken in solid state showed a slightly conductor behavior. It is import to note that these results were recovered at localized and superficial level. On the other hand, the determination of fluorescence emission peaks for the oligo(ether-amide)s showed two absorption bands. The first peak is related to the less electron-donating nature of the amide group and the second is attributed to the polar solvent employed.

All the oligo(ether-amide)s presented an amorphous structure, studied by grazing incident X-ray diffraction (GIXRD). This fact could be originated in the disordered microstructure that adopts the oligomeric chain into the system, which is related to the molecular masses and to the specific structural details of each one. AFM micrographs reveal the material topography at surface level. Thus, the sample that presents the highest hole deepness also shows the highest molecular mass in relation to the relative intensity. This fact is

accompanied by the lowest flexibility and the presence of lateral groups of low volume, which promote the highest packing forces between the chains.

The results suggest that the nature of the lateral groups bonded to the silicon atoms and the incorporation of oxyphenyl units in both monomers; dicarboxylic acid and diamine, modulates the properties of the final material. These modifications promote flexibility and at the same time contribute with aromatic content to the sample. The obtained results are strongly related to the conformational options of the chains and therefore, to the packing forces between them.

Acknowledgements

The authors acknowledge the financial assistance by Fondo Nacional de Investigación Científica y Tecnológica, FONDECYT, through Project 1095151. A. Tundidor-Camba and D. Coll thank CONICYT for a fellowship.

References

1. J. Lin, D.C. Sherrington, *Adv. Polym. Sci.* 1994, 111, 177-219.
2. H.H. Yang, *Aromatic High-Strength Fibers*, Wiley and Sons: New York, 1989.
3. C.P. Yang, J.H. Lin, *J. Polym. Sci. Part A: Polym. Chem.* 1994, 32, 423-433.
4. C.P. Yang, J.H. Lin, *Polymer* 1995, 36, 2607-2614.
5. Z. Rafiee, S. Khalidi, *Polym. Bull.* 2013, 70, 2423-2435.
6. M. Bruma, B.J. Schulz, *Macromol. Sci. Polym. Rev.* 2001, C41, 1-40.
7. J.R. Pratt, W.D. Massey, F.H. Pinkerton, S.F. Thames, *J. Org. Chem.* 1975, 40(8), 1090-1094.

8. L.H. Tagle, C.A. Terraza, A. Leiva, F. Devilat, *J. Appl. Polym. Sci.* 2008, 110, 2424-2431.
9. S.F. Thames, K.G. Panjnani, *J. Inorg. Organomet. Polym.* 1996, 6, 59-94.
10. L.H. Tagle, C.A. Terraza, A. Leiva, N. Yazigi, L. López, *J. Appl. Polym. Sci.* 2010, 117, 1526-1534.
11. R. Chavez, E. Ionescu, C. Fasel, F. Riedel, *Chem. Mat.* 2010, 22, 3823-2825.
12. L.H. Tagle, C.A. Terraza, A. Tundidor-Camba, J. Soto-Salamanca, *Polym Bull.* 2014, 71, 287-300.
13. L.H. Tagle, C.A. Terraza, H. Villagra, A. Tundidor-Camba, *Polym. Bull.* 2011, 67, 1799-1807.
14. L.H. Tagle, C.A. Terraza, P. A. Ortiz, A. Tundidor-Camba, *J. Chil. Chem. Soc.* 2011, 56, 945-947.
15. L.H. Tagle, C.A. Terraza, A. Leiva, D. Coll, *High Perform. Polym.* 2012, 24, 77-84.
16. L.H. Tagle, C.A. Terraza, P. Ortiz, M.J. Rodríguez, A. Tundidor-Camba, A. Leiva, C. González-Henríquez, A.L. Cabrera, U.G. Volkmann, E. Ramos-Moore, *J. Macromol. Sci. A: Pure Appl. Chem.* 2012, 49, 562-570.
17. C. González-Henríquez, L.H. Tagle, C.A. Terraza, A. Barriga-González, U.G. Volkmann, A.L. Cabrera, E. Ramos-Moore, M. Pavez-Moreno, *Polym. Int.* 2012, 61, 197-204.
18. C. González-Henríquez, C.A. Terraza, L.H. Tagle, A. Barriga-González, U.G. Volkmann, A.L. Cabrera, E. Ramos-Moore, M.J. Retamal, *J. Mater. Chem.* 2012, 22, 6782-6791.
19. C.M. González-Henríquez, L.H. Tagle, C.A. Terraza, A. Barriga-González, A.L. Cabrera, U.G. Volkmann, *J. Appl. Polym. Sci.* 2012, 125, 477-487.

20. L.H. Tagle, C.A. Terraza, A. Tundidor-Camba, P.A. Ortiz; *RSC Advances*. 2014, 4, 30197-30210.
21. P. Thiruvassagam, M. Vijayan, *J. Polym. Res.* 2012, 19, 9845-9853.
22. I. Bacosa, E. Hamciuc, M. Cristea, G. Lisa, M. Bruma, *J. Appl. Polym. Sci.* 2012, 124, 1956-1966.
23. C.A. Terraza, L.H. Tagle, A. Tundidor-Camba, C.M. González-Henríquez, P. Ortiz, D. Coll, *Eur. Polym. J.* 2012, 48, 649-661.
24. C.A. Terraza, L.H. Tagle, D. Mejías, A. Tundidor-Camba, P. Ortiz, D. Muñoz, F. Alvarez, C.M. González-Henríquez, *Polym. Bull.* 2013, 70, 773-788.
25. C.A. Terraza, L.H. Tagle, C. Contador, A. Tundidor-Camba, C.M. González-Henríquez, *Polym. Bull.* 2014, 71, 1101-1115.
26. C.A. Terraza, L.H. Tagle, A. Leiva, L. Poblete, F.J. Concha, *J Appl. Polym. Sci.* 2008, 109, 303-308.
27. L.H. Tagle, F.R. Diaz, J.C. Vega, P. Valenzuela, *Eur. Polym. J.* 2003, 39, 407-410.
28. N. Yamazaki, M. Matsumoto, F. Higashi, *J. Polym. Sci. Polym. Chem. Ed.* 1975, 13, 1373-1380.
29. H. Mighani, M. Ghaemy, *Chin. J. Polym, Sci.* 2010, 28, 147-155.
30. C.A. Terraza, L.H. Tagle, F. Concha, L. Poblete, *Design. Mon. Polym.* 2007, 10, 253-261.
31. D. Lin-Vien, N.B. Colthup, W.G. Fateley, J.G. Grasselli, *The Handbook of Infrared and Raman Characteristic Frequencies of Organic Molecules*, Academic Press: New York, 1991, Chapter 9.
32. T. Miyazawa, T. Shimanouchi, S. Mizushima, *J. Chem. Phys.* 1956, 24, 408-418.
33. T. Miyazawa, T. Shimanouchi, S. Mizushima, *J. Chem. Phys.* 1958, 29, 611-616.

34. C.G. Cannon, *Spectrochim. Acta* 1960, 16(3), 302-319.
35. M. Beer, H.B. Kessler, G.B.B.M. Sutherland, *J. Chem. Phys.* 1958, 29(5), 1097-2004.
36. K.W.F. Kohlrausch, *Ramanspektren: Die Spektren. Die Entstehung und Zusammenhang mit der Struktur der Materie*, Abschnitt VI. Akademische Verlagsgesellschaft Becker & Erler: Leipzig, 1943.
37. S.E. Wiberley, S.C. Bunce, W.H. Bauer, *Anal. Chem.*, 1960, 32, 217-221.
38. J.M. Lebas, C. Carrignou-Lagrange, M.L. Josien, *Spectrochim. Acta* 1959, 15, 225-235.
39. S-H. Hu, H-L. S-H, J. Leu, *Synthesis and the structure-property of transparent polyimide films prepared by fluorinated monomers for flexible substrates applications*, IUMRS-ICA, September 19~22, 2011, Taipei, Taiwan.
40. J. Tauc, R. Grigorovici, A. Vancu, *Phys. Status Solidi B*. 1966, 15, 627-637.
42. J. Tauc, *Mat. Res. Bull.* 1968, 3, 37-46.
42. F. Mark, *Optical Properties of Solids*, Oxford University Press Inc: New York, 2001.